THE AMERICAN SOCIETY OF MECHANICAL ENGINEERS
345 E. 47th St., New York, N.Y. 10017

97-GT-454

COMPUTATION OF SEPARATED-FLOW TRANSITION USING A TWO-LAYER MODEL OF TURBULENCE

Elias L. Papanicolaou[1] and Wolfgang Rodi
Institute for Hydromechanics
University of Karlsruhe
76128 Karlsruhe
Federal Republic of Germany

ABSTRACT

A model for predicting transition in flows with separation is presented in this study. The two-layer model of turbulence is employed, along with a suitably defined intermittency function, which takes appropriate values in the laminar-, transitional- and turbulent-flow regions. Correlations derived from measurements are used for this purpose. Two test cases were selected : the flow over a long horizontal body with semi-circular leading edge and the flow over the backward-facing step of small height (expansion ratio of 1:1.01). In the former, oncoming flows with a freestream turbulence level encountered in practical applications was considered (0.2 % - 5.6 %), whereas in the latter the corresponding level was much lower. The Reynolds numbers, based on the diameter in the first case and on the step height in the second, lie in the range of 1600-6600, in which limited numerical investigations were previously available and where bubbles with laminar separation and turbulent reattachment are expected.

The predictions were found to compare well with the corresponding measurements, both in terms of the lengths of the separation and the transition regions and of velocity and turbulence intensity profiles at various streamwise locations. The results show that, for the transition criterion chosen, in all cases transition is completed downstream of the reattachment point and that the rate at which it is completed increases with the freestream turbulence level.

NOMENCLATURE

C_f	=	Skin friction coefficient $= \tau_w/(\rho\, U_\infty^2)$
C_p	=	Pressure coefficient $= (p - p_i)/(\rho\, U_\infty^2)$
D	=	Leading-edge diameter of the body in testcase 1
H	=	Height of the backward-facing step (testcase 2)
H_{12}	=	Shape factor $H_{12} = \delta_1/\delta_2$
J	=	Jacobian of the coordinate transformation matrix, defined as $J = \partial(x,y)/\partial(\xi,\eta)$
k	=	Turbulent kinetic energy, non-dimensionalized by U_i^2
L	=	Length scale of turbulence (dimensionless)
p	=	Pressure
P	=	Dimensionless pressure $P = p/(\rho\, U_i^2)$
Re	=	Reynolds number based on a characteristic length for each testcase (D or H), e.g., $Re = (U_i D \rho)/\mu$
Re_x	=	Local Reynolds number based on the streamwise coordinate x
Re_2	=	Local Reynolds number based on momentum thickness δ_2
Tu	=	Freestream turbulence (%)
u, v	=	Vertical and horizontal cartesian velocity components, respectively
U, V	=	Dimensionless cartesian velocity components $U = u/U_i$, $V = v/U_i$
x, y	=	Vertical and horizontal cartesian coordinate distance, respectively
X, Y	=	Dimensionless cartesian coordinate distances, e.g., $X = x/D$, $Y = y/D$ (or $X = x/H$, $Y = y/H$ for case 2)

Greek Symbols

γ	=	Intermittency function
δ	=	Boundary Layer Thickness
δ_1	=	Displacement Thickness
δ_2	=	Momentum Thickness
ϵ	=	Rate of dissipation of turbulent kinetic energy, non-dimensionalized by U_i^3/D or U_i^3/H
ξ, η	=	Coordinates in the curvilinear (transformed) system
μ	=	Molecular viscosity of air
μ_t	=	Turbulent viscosity
μ_t^*	=	Viscosity ratio $\mu_t^* = \mu_t/\mu$

[1] Present Address : Institute for Thermal Turbomachinery, University of Karlsruhe, 76128 Karlsruhe, Germany

Presented at the International Gas Turbine & Aeroengine Congress & Exhibition
Orlando, Florida — June 2–June 5, 1997

ρ	=	Density of the fluid
$\sigma_k, \sigma_\epsilon$	=	Prandtl number for the turbulent kinetic energy and its rate of dissipation respectively
τ_w	=	Wall shear stress

Subscripts

i	=	Inlet
r	=	Reattachment point
s	=	Separation point
t (or tr)	=	Start of transition
T	=	End of transition
∞	=	Local freestream conditions
$\infty, 6$	=	Freestream conditions 6 mm from the leading edge (reference point for case 1)

INTRODUCTION

The successful numerical prediction of the flow around surfaces or bodies such as airfoils and turbine or compressor blades, depends to a great extent on the ability to account for and adequately simulate the transition from laminar to turbulent flow. Although a large number of experimental observations and quantitative data are available to characterize transition in various flows of practical interest, the numerical predictions are still lagging behind and are mostly limited to simple geometries. As far as transition mechanisms are concerned, one can distinguish between *natural transition* and *bypass transition*, while more recently a third type, the *separated-flow transition* has received increasing attention. The first two apply to boundary layers attached to a surface, while the third one refers to separated shear layer transition.

The different features of each transition type have been described by Mayle (1991). The natural transition is closely related to the development of Tollmien-Schlichting waves in a laminar boundary layer, which is a well known problem in fluid mechanics and has been treated by linear stability analysis (Schlichting, 1979). It normally occurs in flows with low freestream turbulence. Bypass transition is due to the entrainment and subsequent growth of turbulent spots in the laminar boundary layer and occurs at high freestream turbulence levels. Its analytical treatment is based on the turbulent spot theory of Emmons (1951). Separated-flow transition occurs when a laminar boundary layer separates from a surface and a separation hubble is formed. Then a free-shear layer develops, along which the transition takes place. In most cases, the separation bubble is laminar and the flow is turbulent at or soon after the reattachment point, in which case the flow situation can be described as laminar separation -turbulent reattachment.

A large number of computational studies has been presented over the past decades on boundary-layer transition, considering mainly attached flow configurations. Most of them were based on modifications of previously existing turbulence models, and as research in the area of turbulence modelling itself advanced, so did transition modelling. An extensive account of the recent modelling efforts in transition, particularly those made by European researchers, has been presented by Savill (1995). This reflects the activities of the Special Interest Group (SIG) on Transition formed within ERCOFTAC [2]. The most popular approach seems to be the low Reynolds $k-\epsilon$ model, both in a parabolic and an elliptic form, but also integral methods, non-isotropic $k-\epsilon$ models, Reynolds stress models, models including transport equations for intermittency and large eddy simulation have been used among others. All these have been used for computations under a variety of external flow conditions, such as level of freestream turbulence and pressure gradient, the latter of which can have zero or non-zero values and can be of favorable or adverse nature.

In the study of separated-flow transition, the most common configuration has been the leading edge separation bubbles on airfoils. The various methods that have been adopted for this purpose have been classified by Walker et al. (1988) as : a) *Semi-empirical methods*, b) *Viscous-inviscid interactian methods* and c) *Navier-Stokes solutions*, of which the first two classes are the most widely encountered in the literature. An example of semiempirical methods and correlations was offered by the work of Roberts (1980), which aimed at analysing the phenomena associated with leading-edge separation bubbles on airfoils. He discussed in detail the features of the two main types of separation bubbles, namely *short* and *long* bubbles. The short ones have a local effect on the flow and only slightly affect the inviscid flow outside the bubble. Long bubbles on the other hand exhibit a significant interaction with the external flow, so that the pressure distribution modified markedly compared to the inviscid case. He defined four flow regimes based on very low, low, medium and high chord Reynolds numbers which give complete separation, long bubbles, short bubbles and no separation respectively.

Some of the earliest attempts to investigate transition in separation bubbles were based on analytical methods which distinguished between an inviscid region outside the bubble, where potential-flow theory could be employed, and a viscous region inside the bubble where boundary-layer analysis could be used. Thus each region was treated independently and an iterative procedure was followed, during which an attempt was made to match the two results at the interface between the two regions. Among the most representative studies in this area are those by Crimi and Reeves (1976) and Kwon and Pletcher (1979). Both were interested in leading-edge separation bubbles on airfoils and the prediction of the phenomenon of 'bursting', which could lead to stall at a given angle of attack. A constant-thickness airfoil with a cylindrical nose was the configuration used by Arena and Mueller (1980) for low-speed wind tunnel measurements in an attempt to study leading-edge separation bubbles. Different angles of attack, flap angles and chord Reynolds numbers in the range 150,000-460,000 were investigated. Bellows and Mayle (1986) performed heat transfer measurements on a similar body, at Reynolds numbers, based on the diameter, $Re = 80,000, 100,000$ and 120,000 and freestream turbulence level of 0.4 %.

In this study, some of the ideas used in previous efforts to model separation bubbles as described above are employed, in conjunction with a full, elliptic simulation of the flow over a body with a semi-circular leading edge and a backward facing step of

[2] European Research Community On Flow Turbulence And Combustion

small height. The two geometries are shown in Fig. 1. These were proposed in the course of the activities of the ERCOFTAC SIG on Transition mentioned earlier (Savill, 1992). The first flow situation has not been very extensively investigated in the past and only the experimental studies of Arena and Muller (1980), Bellows and Mayle (1986) and Malkiel and Mayle (1996) are on similar flows, but the authors considered higher Reynolds numbers and mostly non-zero angles of attack.

The second testcase, the backward-facing step, has been much more frequently investigated. Many test calculations have been carried out for laminar flow ($Re \leq 800$, based on the step height) and fully turbulent flow ($Re \geq 5000$ or higher), but very few attempts have been made to simulate the flow in the transition regime, such as for instance the studies of Karniadakis et al. (1990) and Kaiktsis et al. (1991). The latter has reported bifurcations to three-dimensional and oscillatory flow patterns at the early stages of transition. The expansion ratios (outlet height/inlet height) associated with the step were in most cases 1.5 or larger. On the other hand, the present value is very close to unity, due to the very small step height, namely 1.012. The step-height Reynolds number is equal to 4095.

Here, both testcases described are simulated numerically in the transitional regime. In both of them laminar separation is expected, with a separation point whose location is either not known in advance (case 1) or is fixed (case 2, step corner). Eventually a fully-turbulent reattached flow is expected. The full elliptic, two-dimensional flow equations are solved, along with a two-layer model of turbulence, where the viscosity is adjusted through an intermittency function in the laminar, transitional and turbulent flow regions. This function is defined in such a manner that previous findings on separated flows can be incorporated into the transition model, thus allowing some elements of the physics of these particular flows to be accounted for. Experimental data for testcase 1 were obtained at the Rolls-Royce Applied Science Laboratory (RRASL), Derby, UK (Coupland, 1995) and for testcase 2 at the Engineering Department of Cambridge University, Camhridge, UK (Savill, 1992).

MATHEMATICAL MODEL

Model Equations

In a two-dimensional, Cartesian coordinate system, the steady equations governing incompressible flow and using the $k-\epsilon$ turbulence model, can be written in the following dimensionless and compact form :

$$\frac{\partial \mathbf{F}}{\partial X} + \frac{\partial \mathbf{G}}{\partial Y} = \frac{\partial \mathbf{F_d}}{\partial X} + \frac{\partial \mathbf{G_d}}{\partial Y} + \mathbf{S} \qquad (1)$$

where F and G are the convective flux vectors, defined as :

$$\mathbf{F} = \begin{bmatrix} \overline{U} \\ \overline{U}\,\overline{U} + \mathrm{P} \\ \overline{U}\,\overline{V} \\ \overline{U}k \\ \overline{U}\epsilon \end{bmatrix} \quad , \quad \mathbf{G} = \begin{bmatrix} \overline{V} \\ \overline{V}\,\overline{U} \\ \mathrm{P} + \overline{V}\,\overline{V} \\ \overline{V}k \\ \overline{V}\epsilon \end{bmatrix} \quad , \qquad (2)$$

$\mathbf{F_d}, \mathbf{G_d}$ are the diffusive flux vectors and S is a source term

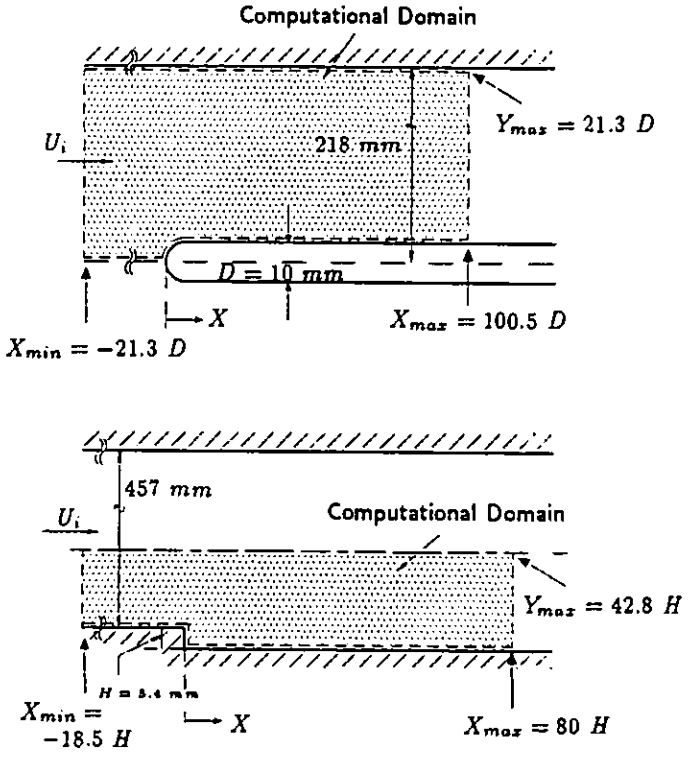

Fig. 1: Schematic of the two testcases with the corresponding significant dimensions. Case 1 : Long horizontal body with semi-circular leading edge (top). Case 2 : Backward-facing step of small height (bottom).

vector. $\mathbf{F_d}$ and S are defined as :

$$\mathbf{F_d} = \frac{1}{Re} \begin{bmatrix} 0 \\ (1+\gamma\mu_t^*)\left(2\frac{\partial \overline{U}}{\partial X}\right) \\ (1+\gamma\mu_t^*)\left(\frac{\partial \overline{U}}{\partial Y} + \frac{\partial \overline{V}}{\partial X}\right) \\ \left(1+\frac{\gamma\mu_t^*}{\sigma_k}\right)\left(\frac{\partial k}{\partial X}\right) \\ \left(1+\frac{\gamma\mu_t^*}{\sigma_\epsilon}\right)\left(\frac{\partial \epsilon}{\partial X}\right) \end{bmatrix} \quad , \quad \mathbf{S} = \begin{bmatrix} 0 \\ 0 \\ 0 \\ S_k \\ S_\epsilon \end{bmatrix} \qquad (3)$$

and $\mathbf{G_d}$ is defined accordingly, whereas :

$$S_k = \gamma P_k - \epsilon \quad , \quad S_\epsilon = C_1\,\gamma P_k \left(\frac{\epsilon}{k}\right) - C_2 \left(\frac{\epsilon^2}{k}\right) \qquad (4)$$

$$P_k \equiv \frac{1}{Re}\mu_t^* \left(\frac{\partial \overline{U}_i}{\partial X_j} + \frac{\partial \overline{U}_j}{\partial X_i}\right)\frac{\partial \overline{U}_i}{\partial X_j} \quad , \quad \mu_t^* = C_\mu \frac{k^2}{\epsilon} Re \qquad (5)$$

The standard values of the $k-\epsilon$ model constants are used : $\sigma_k = 1$, $\sigma_\epsilon = 1.3$, $C_1 = 1.44$, $C_2 = 1.92$, $C_\mu = 0.09$. γ is the intermittency function used to model transition and will be defined below. Since here a two-layer model is employed, the $k-\epsilon$ model is used only in the outer region. In the near-wall region a one-equation model is used as explained below, whereby the ϵ equation is not solved. For computational domains of non-rectangular shape, such as the one in testcase 1, a curvilinear,

boundary-fitted coordinate system (ξ, η) is employed. The chain rule is used for the transformation of the derivatives from the cartesian to the curvilinear system and Eq. 1 can be written as :

$$\frac{\partial \overline{\mathbf{F}}}{\partial \xi} + \frac{\partial \overline{\mathbf{G}}}{\partial \eta} = \frac{\partial \overline{\mathbf{F}}_d}{\partial \xi} + \frac{\partial \overline{\mathbf{G}}_d}{\partial \eta} + \mathbf{J}\,\overline{\mathbf{S}} \qquad (6)$$

Boundary Conditions

In both cases an inlet velocity and an inlet freestream turbulence level are specified. At the outflow, placed sufficiently far from the separation bubble, all streamwise gradients are taken as zero . On the solid surfaces the no-slip conditions are applied. In testcase 1, the computations extend all the way to the opposite wall, where the viscous sublayer is not resolved but wall functions are used. Due to the symmetry of the geometry, only the upper half of the flow is calculated and a symmetry condition is imposed at the symmetry plane upstream of the body. In testcase 2, due to the large distance of the opposite wall in the experiments, the upper boundary is taken midway across the channel height, where symmetry conditions are imposed.

Of utmost importance in transition modelling, are the inlet conditions for the turbulence quantities. For testcase 1, it was specified (Savill, 1992) that the freestream turbulence Tu, under the prevailing zero-pressure-gradient conditions, decays in a power-law fashion, while the dissipation length scale L_ϵ increases with the square-root of the streamwise distance. Depending on the properties of the turbulence-generating grids used in each subcase, suitable constants of the power-law expression were computed, using measured values of freestream turbulence above the body surface that were provided. Once the expressions for Tu and L_ϵ are fully determined, their corresponding inlet values can be determined by upstream extrapolation. The value of dissipation rate at the inlet is in turn obtained from the relationship $L_\epsilon = k^{3/2}/\epsilon$ and the turbulent viscosity at inlet from Eq. 5. In testcase 2, Blasius conditions at the inlet are proposed, along with a measured, given profile for the turbulence intensity, while for the dissipation length scale a profile obtained from the relationship : $L_\epsilon = min[\kappa\ y, 0.085\ \delta]/C_\mu{}^{3/4}$ was recommended (Savill, 1994), where $\kappa = 0.41$ (von Karman's constant) and y is the distance from the bottom surface of the inlet channel.

Two-layer model

The two-layer model as described in the paper by Rodi (1991) is used in the present computations. It is a combination of the standard $k-\epsilon$ model, used in the outer region, and the Norris-Reynolds one-equation model applied in the near-wall region. Since the computations here are carried out in non-dimensional variables, the various realtionships are presented in a dimensionless form. Therefore, in the Norris-Reynolds approach, the turbulent viscosity is given by the following expression :

$$\mu_t^* = Re\ f_\mu\ C'_\mu\ \sqrt{k}\ L \qquad (7)$$

$$\text{where :} \qquad f_\mu = 1 - exp\left(-\frac{Re_y}{A_\mu}\,\frac{25}{A^+}\right)$$

$$Re_y = Re\ \sqrt{k}\ Y_n \quad , \quad L = C_D\ \kappa\ Y_n \qquad (8)$$

and : $C'_\mu = 0.084$, $A_\mu = 50.5$, $C_D = 6.41$, $\kappa = 0.41$. Y_n is the dimensionless distance normal to the wall. Only the k equation is solved in the near-wall region, with the source term S_k of Eq. 4 using the following value of ϵ :

$$\epsilon = \frac{k^{3/2}}{L}\left(1 + \frac{1}{Re}\,\frac{C_\epsilon}{\sqrt{k}\ L}\right) \quad , \quad C_\epsilon = 13.2 \qquad (9)$$

The criterion for switching between inner and outer region modelling is determined by the value $f_\mu \approx 0.95$ (Rodi, 1991) or the boundary layer edge, whichever is attained first as one moves away from the wall. This model has been previously used to compute transitional, attached flows in turbine cascades (Cho et al., 1993). Transition was effected by an empirical relation for changing A^+ from a large value in the laminar flow to $A^+ = 25$ in fully turbulent flow. The start of transition was determined with the empirical formula of Abu-Ghannam and Shaw (1980). Here, the latter procedure is not used, but A^+ is kept constant at $A^+ = 25$ (turbulent flow) and the transition process is controlled instead through the intermittency function γ, as shown in Eqs. 3 and 4 and as will be described below.

Transition Model Parameters

The intermittency function γ, appearing in Eqs. 3- 4 as a multiplication factor for the eddy viscosity, represents the fraction of time during which a flow at the given location is turbulent (Mayle, 1991). The values of γ range from 0, corresponding to laminar flow, to 1, which indicates a fully-turbulent flow. Values between 0 and 1 represent a state of transition from laminar to turbulent flow at a particular point. The rate at which the values of γ increase from 0 to 1 during transition is determined by the rate of the turbulent spot production (Emmons, 1951) and is generally of exponential nature. Different investigators have proposed different parameters that control this exponential growth and presented γ as a one-dimensional function of the streamwise coordinate, corresponding to values near the wall (near-wall intermittency) (Mayle, 1991). Such expressions, accompanied by correlations for the onset of transition and the extent of the transition region may then be used for modelling the flow in the transition region.

Here, the following expression is used for intermittency :

$$\gamma(x) = 1 - exp\left[-G(x - x_{tr})\int_{x_{tr}}^{x}\frac{dx}{U_\infty}\right] \qquad (10)$$

$$\text{where :} \qquad G = \frac{exp(0.99\ Tu)}{100}\,\frac{{U_\infty}^3}{\nu^2}\,Re_{2,tr}{}^{-8/3} \qquad (11)$$

proposed by Rodi and Schönung (1987) as an extended version of the work by Chen and Thyson (1971). This expression involves the value of the Reynolds number $Re_{2,tr}$ based on the momentum thickness at the transition point and the coordinate of the transition point x_{tr}. $Re_{2,tr}$ is obtained at each streamwise location from the following correlation :

$$Re^2_{2,tr} = \left(1 + \frac{0.05}{exp(0.365\ Tu)}\right)\ Re^2_{2,sep} + \frac{17000}{exp(0.509\ Tu)} \qquad (12)$$

The coordinate at the start of transition x_{tr} is taken as the location at which the local value of Re_2 exceeds the value of $Re_{2,tr}$ computed from Eq. 12. The above expression has been developed by Rodi and Schönung (1987), by modifying previous published

correlations which incorporated the coordinate of the separation point (see, for instance, Kwon and Pletcher (1979)). These were based on the assumption that transition starts when the maximum displacement thickness due to separation is attained, which coincides with the end of the constant pressure region. Rodi and Schönung (1987) introduced the momentum-thickness Reynolds number instead of the local Re in the correlations, along with the effect of the freestream turbulence. The various coefficients involved were obtained by optimization, based on the experimental data of Gotthardt (1983) and Haas et al. (1987). As can be observed, this correlation involves the Reynolds number at the separation point and therefore it is particularly suited for separated flows. The good prediction of the separation point and the accurate estimation of the various boundary layer thicknesses are essential to the successful use of this model.

COMPUTATIONAL SCHEME

Main Features

The code FAST-2D [3] (Zhu, 1991a) was used for the present computations. This was developed at the Institute for Hydromechanics, at the University of Karlsruhe, Germany over the past decade by various researchers. A detailed description of it, or more strictly its three-dimensional version, is given in the paper by Majumdar et al. (1992). Its main features consist of a control-volume approach, discretization of Eq. 6 in a generalized, non-orthogonal coordinate system, where the cartesian velocity components are used to describe the flow field. The code is based on the pressure-correction algorithm SIMPLE (Patankar, 1980) and its variant SIMPLEC (Van Doormal and Raithby, 1984), the latter of which was used in the present computations. A non-staggered grid arrangement and the momentum interpolation procedure of Rhie and Chow (1983) is used to avoid the checkerboard splitting. The convective terms are discretized using the HLPA scheme (Hybrid Linear / Parabolic Approximation) described by Zhu (1991b). This is a higher-order, bounded scheme, with good stability properties.

Computational Domain and Grid

The extent of the computational domains for both cases is shown in Fig. 1. For the first testcase, the horizontal surface of the body is equal to exactly 100 diameters, while vertically the domain is extended up to the wind tunnel wall, as specified by the experimental setup. For the step, the distances chosen (80H downstream of the step, 42.8H vertically) were eventually found to be sufficient to avoid any undesirable boundary influence on the solution, after several possibilities were tested. At the mid-height of the test channel a symmetry condition was employed. The grids used in the computations for the two testcases are shown in Fig. 2. After several attempts, the final grid dimensions which were considered necessary for a good resolution of the body surface in case 1 were 142 × 102, with 142 points in the streamwise direction. The grid spacings were stretched in the streamwise direction towards the curved surface of the body. In the second testcase, the same number of points was used. Here the emphasis in the stretching of the grid was towards the shear layer expected to develop as the flow separates at the corner.

[3] F-low A-nalysis S-imulation T-ool of 2-D

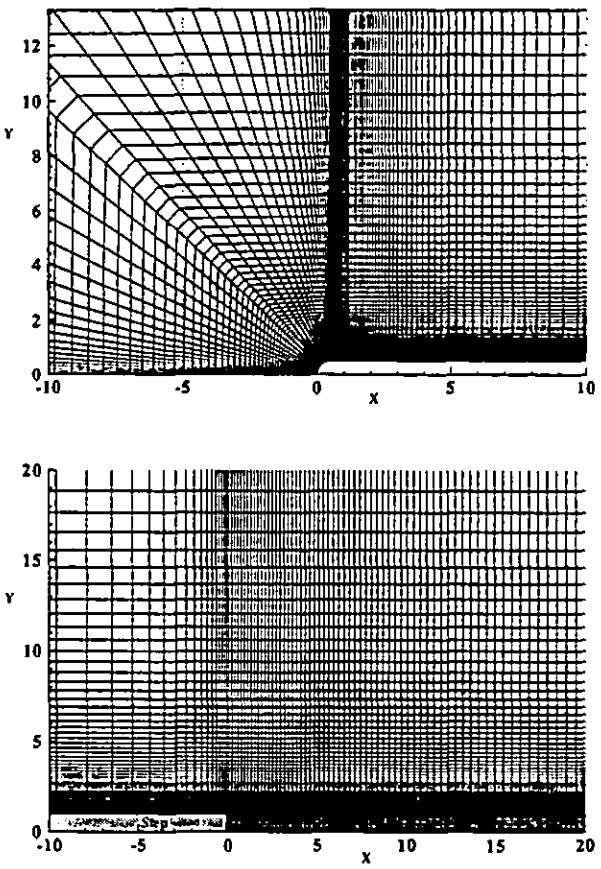

Fig. 2: Section of the computational grid for the two testcases shown in Fig.1.

Therefore stretching in both the upward and downward direction was used towards the approximate vertical location of the shear layer. In both cases, the grid dimensions and stretching factors used yielded values of Y^+ at the first grid point from the wall of the order of 1 or less, therefore ensuring a fair amount of grid points inside the boundary layers.

Procedure and stability considerations

The velocity components and the pressure were initialized with the laminar flow solution obtained on the same configuration for a sufficiently lower Reynolds number. The computations proceeded until the root-mean square residuals of all variables were reduced to the order of 10^{-5} or less. During the early attempts, it became evident that the numerical procedure tended to become unstable, especially in testcase 2 where the level of freestream turbulence is very low, and multiple separation bubbles developed. It was soon realized that this was due to setting $\gamma = 0$ in the laminar-flow regions. It was therefore found necessary to avoid letting the turbulent viscosity go to zero in the diffusion terms of Eq. 3 in these regions. The intermittency was instead set to 1 in the diffusion terms (but not in the production terms) in the laminar region in the free stream. A small amount of diffusion was also allowed in the laminar boundary layer, by setting γ to a small value, in the range 0.1-0.2, again in the diffusion terms only. Such values were found to be adequate for numerical stability without affecting the overall results, after

experimentation in several cases with various flow conditions, and they were maintained in that range in all subsequent calculations. This practice was also directed by physical reasoning, since otherwise the diffusion of freestream turbulence into the laminar boundary layer would not have been properly accounted for and since it was also known from the measurements that the oncoming flow carried some amount of turbulence with it, both in the free stream and within the laminar boundary layer before transition.

RESULTS AND DISCUSSION

Testcase 1

The flow conditions which were specified for the body with the semi-circular leading edge are listed in Tahle 1. Each subcase is characterized by a letter 'a-f'. Results for all these subcases could not be presented here due to limited space, but the reader is referred to the report by Papanicolaou (1996) for additional results. Here only 1c and 1f are presented in detail.

Results for $U_i = 5$ m/s, Re = 3293 . In Fig. 3 a typical streamline plot is shown. A quite sizeable separation bubble is present, whose size varies from case to case, as will be demonstrated below. The bubble in case 1c, for instance, had a length roughly equal to 2.3 diameters. The separation point is located slightly upstream of the beginning of the horizontal surface of the body. On the same figure, the streamwise intermittency distribution $\gamma(X)$ is also shown. The predicted transition point is located at $X_t = 2.41$ diameters from the leading edge. This corresponds to a distance equal to 85% of the bubble length. The transition ends at a streamwise coordinate of $X_T = 2.83$, yielding a total length of transition equal to 0.42 diameters. The predicted transition behavior appears to be more in accord with the findings of Walker (1992), than those of Mayle (1991), as far as the end-of-transition point is concerned. More specifically, here the transition process seems to be completed downstream of the reattachment point, i.e., the flow is not fully-turbulent at reattachment. However, the end-of-transition locations here, obtained for $\gamma = 0.99$, were the outcome of a stricter transition criterion which used the intermittency values computed as a function of the freestream value of Tu (Eq. 11). Since assuming a crossflow variation for the intermittency was outside the scope of this work, using the freestream conditions to represent each streamwise coordinate was the most convenient choice. It is expected that by taking into account a crossflow distribution of intermittency, such as those measured recently by Malkiel and Mayle (1996) or Hazarika and Hirsch (1996), and by using the local peak value of the intermittency to monitor transition instead, an earlier end-of-transition point X_T will be found. Unfortunately, based on the available data, there is no clear experimental evidence regarding the relative position of the end-of-transition and reattattachment points.

The various subcases corresponding to an inlet velocity of 5 m/s can be compared in terms of the values shown in Table 1. The separation point varies only slightly with the freestream turbulence level Tu, while the reattachment point and the start-, end-of-transition points are shifted further upstream with an increase in Tu. In Fig. 4, for case 1c, calculated and measured values of the boundary-layer thickness δ, maximum velocity of the external flow U_{max} and shape factor are plotted versus the horizontal coordinate X. δ is defined as the wall distance where the velocity is 0.99 of the maximum value. The comparison with the experimental results can be seen to be good, both in terms of δ and maximum velocity. The plot of U_{max} indicates that the effect of the bubble extends down to about five body diameters from the leading edge. The shape factor plot exhibits a sharp peak typical of a separation bubble, (somewhat excessive in the calculations) before an asymptotic value of 1.44 is attained. This is very close to the value reported by Schlichting (1979) for turbulent boundary layers on a flat plate. The comparison with the measurements appears fairly good, except for some under-prediction of U_{max} in the separation region.

In Fig. 5 additional comparisons with measured data are shown, this time for the skin friction coefficient C_f and the Reynolds number Re_2 based on the momentum thickness, both plotted against the local Reynolds number Re_x. The bubble location in the plot of C_f is indicated by zero values in the measurement data and by negative values in the computations. It can be readily observed that the predicted length and location for the separation bubble agrees quite well with the measurements. The analytical result for the variation of C_f in a turbulent boundary layer over a flat plate, given by a $Re_x^{-0.2}$ relationship (Schlichting, 1979), is also plotted and coincides with the numerical results in the fully turbulent region. The flow behavior in the laminar region is very different from that of a boundary layer over a flat plate, both due to the curvature and the separated region; therefore it would be meaningless to include the analytical result for C_f in the laminar region. Fig. 5 includes a graphical representation of the relationship between Re_2 and Re_x, as predicted numerically, in comparison with the analytical result for a flat plate. This can be obtained using the corresponding expression for δ_2 (Schlichting, 1979) and indicates a $Re_x^{0.8}$ dependence. In the laminar region the corresponding result is $Re_x^{0.5}$ but, for the same reasons as discussed for C_f, the laminar-flow correlation is not shown as not applicable. However, Fig. 5 shows clearly that, as the turbulent regime establishes, the analytical curve is asymptotically approached by the numerical results.

Fig. 6 compares predicted velocity profiles for case 1c with the corresponding measured ones, at several streamwise distances from the leading edge. The region of reversed flow can be observed in the first three profiles and the comparison is generally good, except for some indication of delayed reattachment. For the same streamwise locations, Fig. 7 compares predicted turbulence intensity profiles for case Ic with the corresponding measured values. The comparison is reasonably good for most profiles. In the last profile, an underprediction of the maximum value of the intensity is observed, which is a known shortcoming of the Norris-Reynolds model and it is due to an overestimation of ϵ (see Rodi et al., 1993). Equally good results were also obtained for the other three values of freestream turbulence listed on Table 1 and corresponding to $U_i = 5$ m/s. The transition was found to be very abrupt for the highest value of Tu and the length of the bubble the smallest of all cases (roughly 1.5 diameters). For the lowest value of Tu, the transition process was slow, but the length of the bubble not significantly affected.

Table 1: Flow conditions and computed separation-transition data for testcase 1

Case	U_i (m/s)	Re	$Tu_{\infty,\delta}$ (%)	X_s	X_T	X_t	X_T
a	5	3293	0.17	0.448	3.247	3.159	6.695
b	5	3293	0.63	0.466	2.913	2.412	3.336
c	5	3293	2.31	0.485	2.759	2.169	2.834
d	5	3293	5.56	0.466	2.005	1.854	2.058
e	2.5	1646.5	2.30	0.500	3.829	4.158	5.495
f	10	6586	2.50	0.448	1.550	1.181	1.953

By reducing the inlet velocity to 2.5 m/s (case 1e), and at the same value of Tu as for case 1c, a longer bubble was obtained and a significantly delayed start of transition.

Results for $U_i = 10$ m/s, $Re = 6586$. The results that follow are for testcase 1f, which has a similar value of freestream turbulence as in case 1c (2.5 %), but a higher velocity, namely 10 m/s. The corresponding streamline plot for this case is shown in Fig. 8 and shows that the length of the bubble ($1.1D$) is much smaller than for case 1c. Transition starts therefore much earlier, but the total length of the transition region (approximately 0.7 diameters) is not significantly different from case c, indicating that it is mainly dependent on the freestream turbulence level and not so much on the Reynolds number.

Figs. 9 and 10 show the various boundary layer quantities that were previously presented for case 1c. Again, overall good agreement can be observed. In particular the plot of C_f shows a very good prediction of the reattachment point. The Re_2 vs. Re_x plot shows again the attainement of turbulent flow conditions at increasing Re_x when compared with the analytical curve. The velocity profiles and turbulent intensities for this case verified once again the good prediction of the reattachment point and exhibited a good overall agreement. In Fig. 11 the pressure coefficients are plotted along the separation and transition regions for cases 1c and 1f. The features typical of a separation bubble, such as a region of constant pressure followed by a downstream region of pressure recovery (Mayle, 1991), can be identified in both cases. The plots further indicate that the start of transition almost coincides with the end of the constant pressure region, as pointed out by Kwon and Pletcher (1979). The pressure recovery is also shown to be complete at the reattacbment point.

To summarize, good comparisons with the measured values were obtained for all six cases shown on Table 1. Some discrepancies were observed only in the prediction of turbulence intensities for the smalest value of the freestream turbulence, $Tu_\infty = 0.17$ % (case 1a), and for the smallest value of the inlet velocity, $U_i = 2.5$ m/s (case 1e). Clearly, some experimentation with alternative values of the parameters involved in Eqs. 11 and 12 would be necessary to produce a more universal model, but this was considered outside the scope of the present work.

Comparisons with experimental correlations

The lengths of separation and transition regions for all six computed cases 1a-1f were subsequently compared against each other in a more systematic way. By using the distances X_s, X_t and X_T listed on Table 1 one can calculate and plot three suitably defined Reynolds numbers $Re_{s,T}$, $Re_{s,t}$ and Re_{LT} , often used to characterize transition, vs. the momentum-thickness Reynolds number at the separation point $Re_{2,s}$. For instance, $Re_{s,T}$ is computed as :

$$Re_{s,T} = \frac{u_s\,(x_T - x_s)\,\rho}{\mu} = Re\; U_s\,(X_T - X_s) \qquad (13)$$

and similarly the other two numbers. In this manner, plots similar to those presented by Mayle (1991) are constructed and shown in Fig. 12. Tbe correlations proposed by Mayle (1991) and Walker (1992) are also included in this figure. The values of $Re_{2,s}$ appearing here represent a relatively narrow band compared to the results plotted by Mayle (1991) and therefore a new correlation cannot be derived based on the present data. However, one can see that tbe computed values of $Re_{s,T}$ (Fig. 12a) are in reasonable agreement with the correlation of Mayle for long bubbles. There is however one data point which falls exactly on the correlating line for short bubbles and this corresponds to the highest value of Tu used (5.56 %) ; for this value the transition is completed shortly after reattachment. Fig. 12b is also showing the data points to be closer to the correlating line of Mayle (1991) for $Re_{s,t}$ for long bubbles. The short bubble correlation is also plotted and cases (d) and (f), where tbe bubbles are indeed short, are tbe closest to it. Both correlations have a $Re_{2,s}^{0.7}$ dependence, but are multiplied by a different factor. In Fig. 12c, the values of Re_{LT} are plotted against two different correlations, one proposed by Mayle (1991), valid for both short and long bubbles and suggesting a $Re_{2,s}^{0.7}$ dependence and another one by Walker (1992) where the dependence is $Re_{2,s}^{1.5}$. Interestingly enough, although qualitatively this study agrees more with the findings of Walker (1992) as far as tbe end-of-transition is concerned, the present results seem to agree quantitatively better with the correlation of Mayle (1991) for Re_{LT}, except for one data point, corresponding to the highest freestream turbulence level (5.56 %). Although the correlations of Mayle (1991) where derived from experimental data corresponding to low freestream turbulence levels (0.2-0.5 %), here a good agreement is observed in the range 0.63-2.5 % (cases b,c,e and f).

Testcase 2

Although experimental data were available in tbis case for three different Reynolds numbers (based on the inlet velocity), Re = 1830, 2535 and 4095 (Savill, 1994), with essentially the same freestream turbulence level Tu of the order 10^{-2} %, only the case with the highest Reynolds number (Re = 4095) could be calculated because of numerical instabilities encountered at this low Tu. In Fig. 13 the streamline plot for this case is shown, along with the corresponding streamwise distribution of the intermittency function. The computed flowfield is characterized

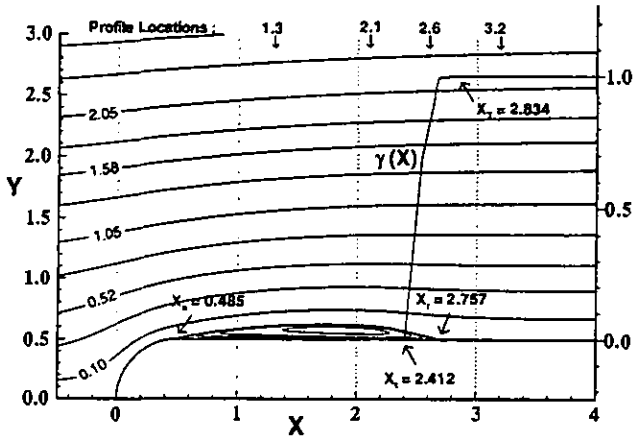

Fig. 3: Streamlines and intermittency distribution $\gamma(X)$ for case 1c ($U_i = 5\ m/s$, $Tu_{\infty,6} = 2.31\ \%$.)

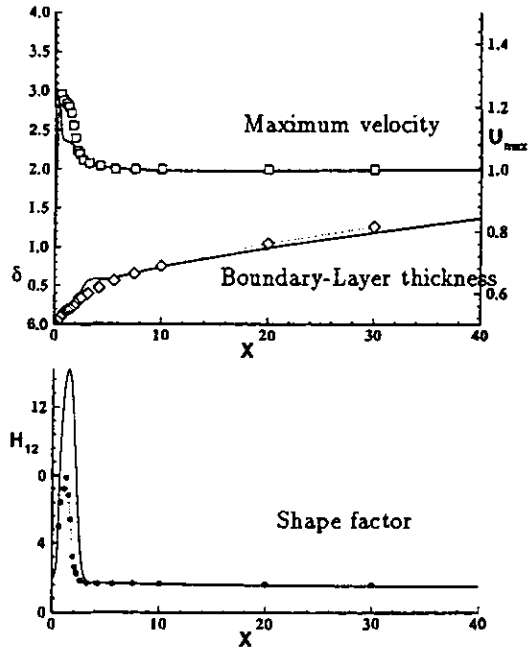

Fig. 4: Numerical (solid lines) against experimental results (points) vs. X for case 1c.

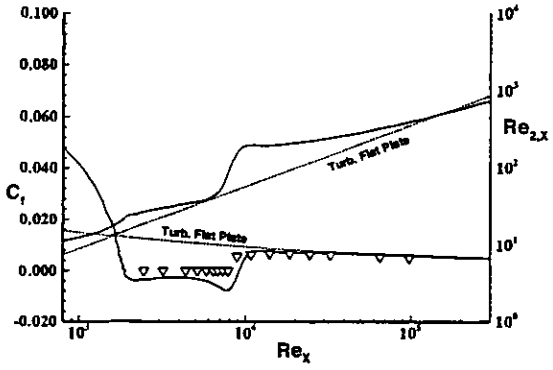

Fig. 5: Numerical (solid lines) vs. experimental results (points) and flat-plate correlations (dashed lines) for case 1c. Skin friction coefficient C_f and local Re_2 are both plotted vs. Re_x.

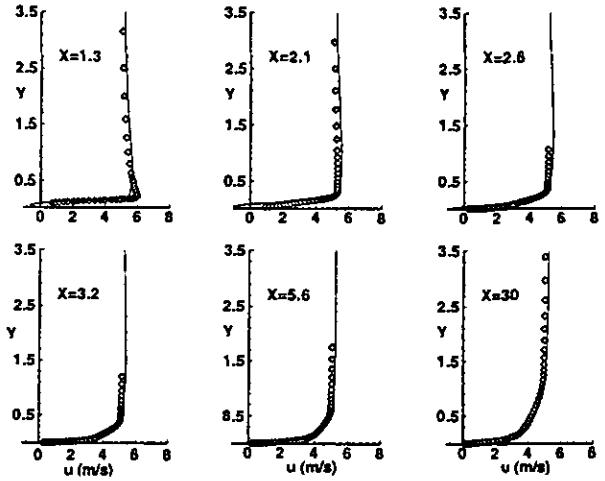

Fig. 6: Numerical (lines) vs. experimental (points) velocity profiles for case 1c.

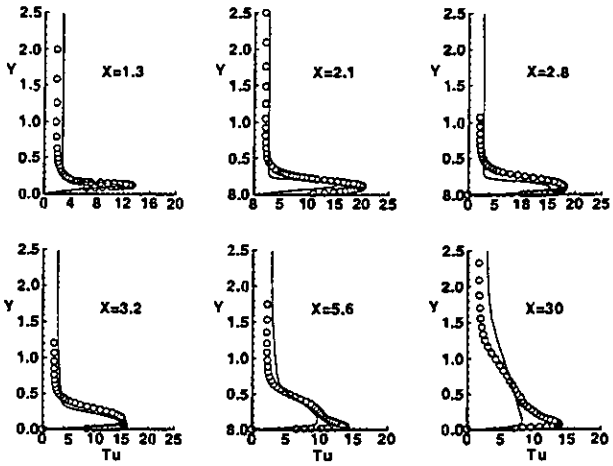

Fig. 7: Turbulence Intensity $\sqrt{\overline{u'^2}}/U_i$ profiles (%) for case 1c

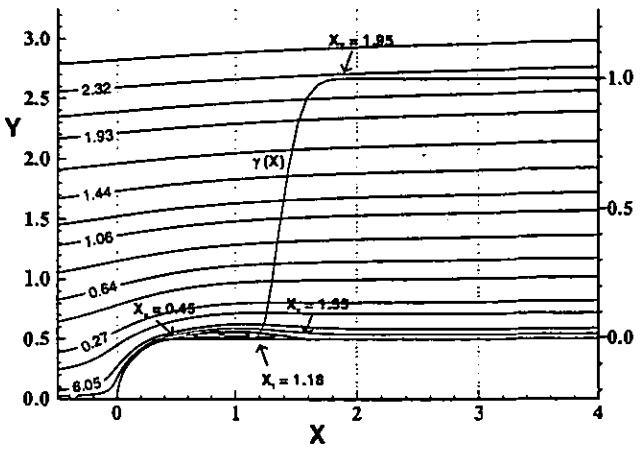

Fig. 8: Streamlines and intermittency distribution $\gamma(X)$ for case 1f ($U_i = 10\ m/s$, $Tu_{\infty,8} = 2.5\ \%$.)

by a relatively long separation bubble (9.54 step heights) immediately donwstream of the step, with a small secondary eddy at the foot of the step. The transition process appears to be relatively slow, a fact that was to be expected considering the very low freestream turbulence level of the oncoming flow. Transition starts at about 4.8 step heights downstream of the step and is completed at a distance of about 18.4 step heights.

The experimental data available for this testcase were in terms of streamwise varying values of the momentum thickness, the maximum velocity of the external flow and the shape factor. In Fig. 14 these quantities are compared with the predicted values along the streamwise distance x/H. The agreement is very good for all three quantities and the extent of the separated region is well predicted. Fig. 15 shows the variation of the skin friction coefficient and Reynolds number based on the momentum thickness. No experimental data were provided for these two quantities and the results are only compared with the analytical flat-plate boundary layer correlations. What can be observed is that the reattached shear layer in this testcase deviates somewhat from the results for turbulent flow over a flat plate.

In Fig. 16 velocity profiles are compared at several streamwise locations downstream of the step with the experimental ones. The experimental data in the first two profiles (separation region) are given as zero or constant, positive values, i.e., no negative velocities were measured. Generally the agreement is good, except for some indication of early reattachment in the numerical results. In Fig. 17 the corresponding turbulence intensities, both numerical and experimental are shown, at the same streamwise locations as the velocities. It can be observed that there is some overprediction of the intensity values at the first station but gradually the numerical values approach the experimental ones. The transition process appears to be very rapid at its early stages in the numerical predictions.

CONCLUSIONS

A computational approach based on a two-layer turbulence model and an empirical intermittency function was presented for calculating transition in separated flows. Two testcases were investigated, one involving flow separation due to curvature and the other one due to sudden expansion (step). The transition process was modelled by means of an intermittency function defined through empirical correlations, based on experimental data. These allowed for the effect of separation to be included in the modelling. The results appear promising as for a relatively wide range of external flow conditions (freestream velocity, level of turbulence) corresponding to values of practical interest in turbomachinery flows, generally good agreement with experimental data was obtained. This can be said both for global quantities such as separation length and location of transition, as well as for local velocity and turbulent intensity profiles.

The model behaved better for freestream turbulence levels in the range 0.6 %-5.6 %, but has been tested also for levels one order of magnitude lower, where it still produced reasonably good results. This study has proven that the intermittency function can be used in several ways in transition modelling, such as for instance in combination with the two-layer model used here, and can lead to successful predictions, but it is necessary to handle with care the laminar-flow regions where this function vanishes, to obtain numerically stable computations.

Available correlations for separated flows based on experimental data such as the ones used here can provide valuable inputs to transitional modelling. However, further experimentation with the various parameters involved in such correlations is needed in order to improve the universality of the models. It is also necessary to investigate additional effects such as rotation or buoyancy and to compute more realistic blade configurations.

ACKNOWLEDGMENTS

This work was sponsored by the German Federal Ministry of Research and Technology through program TURBOTECH, under contract No. 0326801G. Many thanks are due to Dr. Mark Savill of Cambridge University, Cambridge UK for his valuable work in the ERCOFTAC Transition SIG and for providing the experimental results for testcase 2 and to Dr. John Coupland from the Rolls-Royce Applied Sciences Laboratory, Derby, UK, for providing us with the experimental data for testcase 1.

REFERENCES

Abu-Ghannam, B.J. and Shaw, R., 1980, "Natural transition of Boundary Layers- The effects of turbulence, pressure gradient, and flow history", *J. of Mech. Engg. Science*, Vol. 22, No. 5, pp. 213-228.

Arena, A.V., and Mueller, T.J., 1980, "Laminar separation, transition and turbulent reattachment near the leading edge of airfoils", *AIAA J.*, Vol. 18, No. 7, pp. 747-753.

Bellows, W.J., and Mayle, R.E., 1986, "Heat Transfer Downstream of a Leading Edge Separation Bubble", *ASME J. of Turbomachinery*, Vol. 108, pp. 131-136.

Chen, K.K., and Thyson, N.A., 1971, "Extension of Emmons' spot theory to flows on blunt bodies", *AIAA J.*, Vol. 9, No. 5, pp. 821-825.

Cho, N.-H., Liu, X., Rodi, W., and Schönung, B., 1993, "Calculation of wake-induced unsteady flow in a turbine cascade", *ASME J. of Turbomachinery*, Vol. 115, pp. 675-686.

Coupland, J., 1995, "Transition modelling for tubromachinery flows", ERCOFTAC Bulletin, No. 24, pp. 5-8, 1995.

Crimi, P., and Reeves, B.L., 1976, "Analysis of leading-edge separation bubbles on airfoils", *AIAA J.*, Vol. 14, No. 11, pp. 1548-1555.

Emmons, H.W., 1951, "The laminar-turbulent transition in a boundary layer-Part I", *J. of the Aeronautical Sciences*, Vol. 18, pp. 490-498.

Gotthardt, H., 1983, Theoretische und experimentele Untersuchungen an ebenen Turbinengittern mit Pfeilung und V-Stellung. Dissertation, Universität Braunschweig.

Haas, W., Rodi, W., Schönung, B., Swamy, N.V.C., 1987, "Experimentelle Untersuchung von lokalen Ablöseblasen an Gasturbinenschaufeln", *Z. Flugwiss. Weltraumforschung*, Vol. 11, pp. 261-270.

Hazarika, B.K., and Hirsch, C., 1996, "The effect of Reynolds number on the behaviour of a leading edge separation bubble", ASME Paper No. 96-GT-410.

Karniadakis, G.E., Orszag, S.A., and Yakhot V., 1990, "Large-Eddy/RNG simulation of flow over a backward-facing step ", in *Engineering Turbulence Modelling and Experiments*,

W. Rodi and E.N. Ganić (eds.), pp. 269-278, Elsevier, New York.

Kaiktsis, L., Karniadakis, E.M. and Orszag, S.A., 1991, "Onset of three-dimensionality, equilibria, and early transition in flow over a backward-facing step", *J. of Fluid Mech.*, Vol. 231, pp. 501-528.

Kwon, O.K., and Pletcher, R.H., 1979, "Prediction of incompressible separated boundary layers including viscous-inviscid interaction", *ASME J. of Fluids Engg.*, Vol. 101, pp. 466-472.

Majumdar, S., Rodi, W. and Zhu, J., 1992, "Three-dimensional finite-volume methods for incompressible flows with complex boundaries", *ASME J. of Fluids Engg.*, Vol. 114, pp. 496-503.

Malkiel, E., and Mayle, R.E., 1996, "Transition in a Separation Bubble", ASME J. of Turbomachinery, Vol. 118, pp. 752-759.

Mayle, R.E., 1991, "The role of laminar-turbulent transition in gas turbine engines", *ASME J. of Turbomachinery*, Vol. 113, pp. 509-537.

Papanicolaou, E., 1996, "Computation of Separated-Flow Transition Using a Two-Layer Model of Turbulence", Rep. No. 733, Institute for Hydromechanics, University of Karlsruhe, Germany.

Patankar S.V., 1980, *"Numerical Heat Transfer and Fluid Flow"*, Hemisphere, Washington D.C.

Roberts, W.B., 1980, "Calculation of laminar separation bubbles and their effect on airfoil performance", *AIAA J.*, Vol. 18, No. 1, pp. 25-825.

Rhie, C.M., and Chow, W.L., 1983, "Numerical study of the turbulent flow past an airfoil trailing edge separation", *AIAA J.*, Vol. 21, No. 11, pp. 1525-1532.

Rodi, W. and Schönung, B., 1987, "Interaktives-Inverses Grenzschichtverfahren zur Berechnung von lokalen Ablöseblasen an Turbinenschaufeln", *Z. Flugwiss. Weltraumforschung*, Vol. 11, pp. 271-280.

Rodi, W., 1991, "Experience with two-layer models combining the $k-\epsilon$ model with a one-equation model near the wall", AIAA Paper No. 91-0216, presented at the 29th Aerospace Sciences Meeting, Reno, Nevada.

Rodi, W., Mansour N.N. and Michelassi, V., 1993, "One-Equation Near-Wall Turbuleuce Modelling With the Aid of Direct Simulation Data", *ASME J. Fluids Engineering*, Vol. 115, pp. 196-205.

Savill, A.M., 1992, "A T3 Test Case Project Report - Predicting Transition Induced by Free-Stream Turbulence", presented at the IAHR/ERCOFTAC Turbulence Modelling SIG Seminar, Delft, The Netherlands.

Savill, A.M., 1994, T3D Test Case Problem Specification (private communication).

Savill, A.M., 1995, "A Summary report on the COST ER-COFTAC Transition SIG project evaluating turbulence models for predicting transition", ERCOFTAC Bulletin No. 24, pp. 57-61.

Schlichting, H., 1979, "Boundary Layer Theory", McGraw-Hill, New York.

Van Doormal, J.P. and Raithby, G.D., 1984, "Enhancements of the SIMPLE Method for Predicting Incompressible Fluid Flows", *Num. Heat Transfer*, Vol. 7, pp. 147-163.

Walker, G. J., Subroto, P.H., and Platzer, M.F., 1988, "Transition modeling effects on viscous/inviscid interaction of low Reynolds number airfoil flows involving laminar separation bubbles", ASME Paper No. 88-GT-32, presented at the Gas Turbine and Aeroengine Congress, Amsterdam, The Netherlands.

Walker, G. J., 1992, "The role of laminar-turbulent transition in gas turbine engines : a discussion", ASME Paper No. 92-GT-301, presented at the Int. Gas Turbine and Aeroengine Congress and Exposition, Cologne, Germany.

Zhu, J., 1991a, "FAST-2D : A computer program for numerical simulation of two-dimensional incompressible flows with complex boundaries", Rep. No. 690, Institute for Hydromechanics, University of Karlsruhe, Germany.

Zhu, J., 1991b, "A low-diffusive and oscillation-free convection scheme", *Comm. in Applied Num. Methods*, Vo. 7, pp. 225-232.

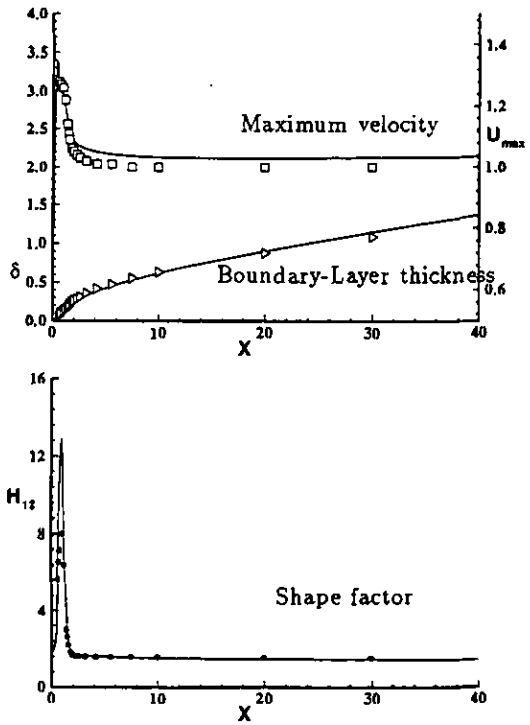

Fig. 9: Numerical (solid lines) against experimental results (points) vs. X for case 1f.

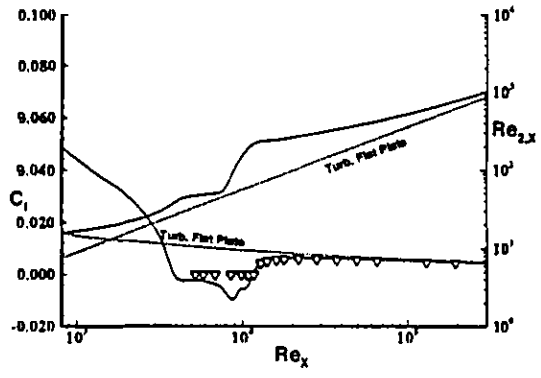

Fig. 10: Numerical (solid lines) vs. experimental results (points) and flat-plate correlations (dashed lines) for case 1f. Skin friction coefficient C_f and local Re_2 are both plotted vs. Re_x .

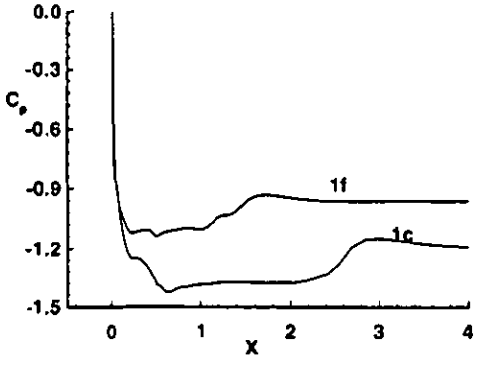

Fig. 11: Pressure Coefficient C_p vs. X for testcases 1c ($X_t = 2.41$) and 1f ($X_t = 1.18$).

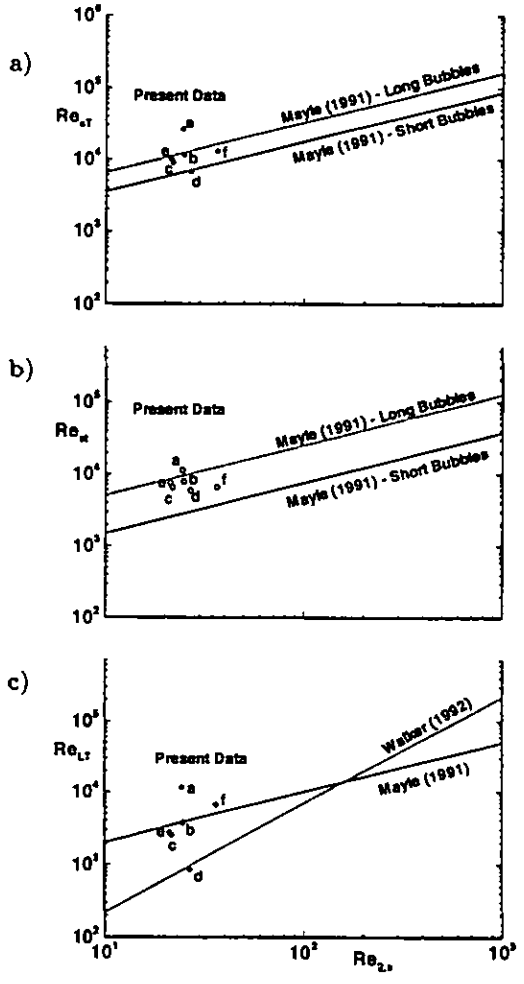

Fig. 12: Separation-bubble data for case 1 vs. $Re_{2,s}$ and against available correlations. The ordinate Re is expressed in terms of : a) The length of the constant-pressure region ($Re_{s,T}$), b) the distance between separation and transition points (Re_{st}), c) the length of the transition region (Re_{LT}).

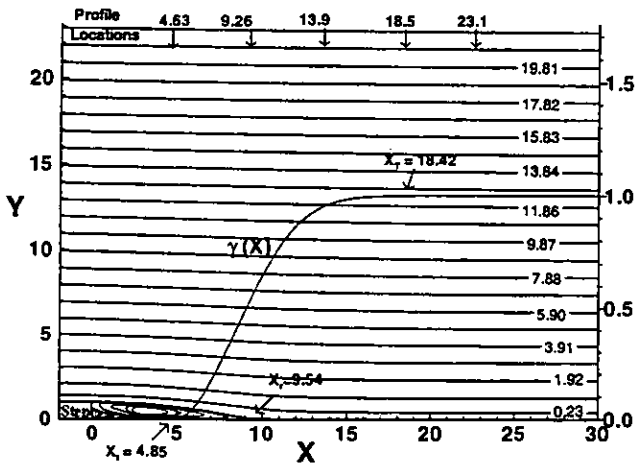

Fig. 13: Streamlines and intermittency distribution for testcase 2 ($U_i = 11.38\ m/s$, $Tu_\infty = 0.011\ \%$.)

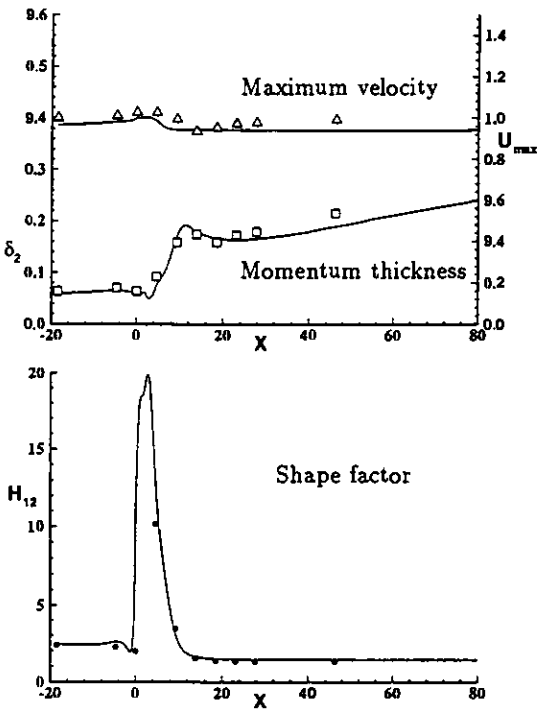

Fig. 14: Numerical (solid lines) against experimental results (points) vs. X for testcase 2.

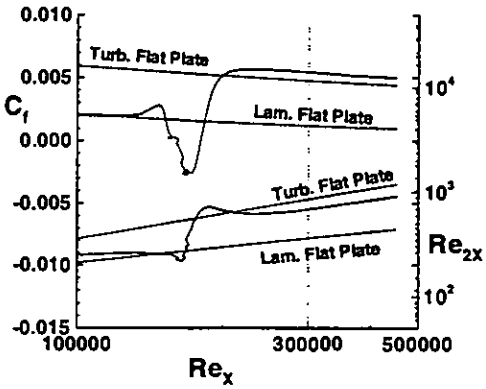

Fig. 15: Numerical results (solid lines) vs. Re_X and against flat-plate correlations (dashed lines) for testcase 2. Skin friction coefficient and momentum-thickness Reynolds number.

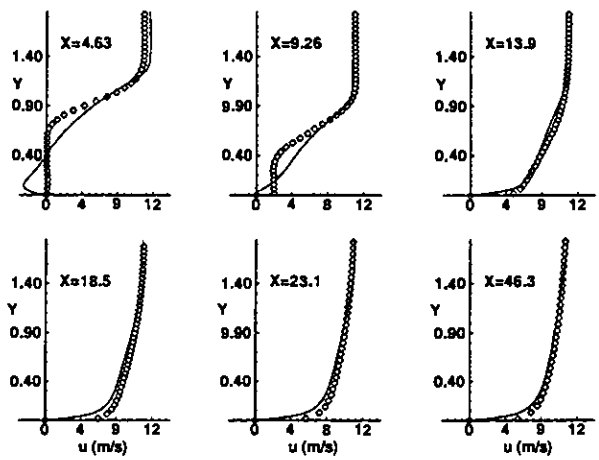

Fig. 16: Numerical (lines) vs. experimental (points) velocity profiles downstream of the step for testcase 2.

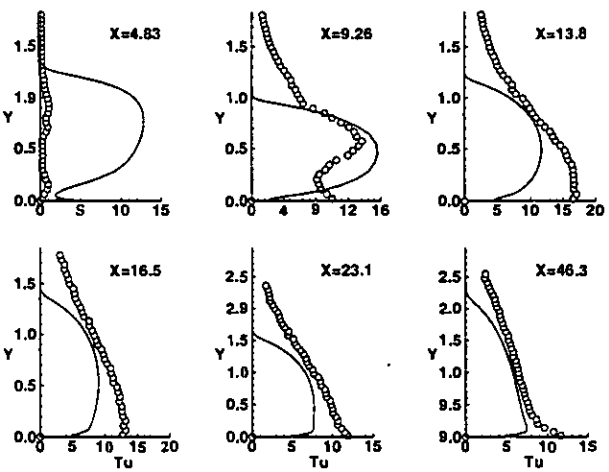

Fig. 17: Turbulence Intensity $\sqrt{\overline{u'^2}}/U_i$ profiles (%) downstream of the step for testcase 2.